*Earth and Planetary Science Letters*, 104 (1991) 440–454
Elsevier Science Publishers B.V., Amsterdam

[DT]

# Cosmic ray produced $^{10}$Be and $^{26}$Al in Antarctic rocks: exposure and erosion history

K. Nishiizumi [a], C.P. Kohl [a], J.R. Arnold [a], J. Klein [b], D. Fink [b] and R. Middleton [b]

[a] *Department of Chemistry, 0317, University of California, San Diego, La Jolla, CA 92093-0317, USA*
[b] *Tandem Accelerator Laboratory, University of Pennsylvania, Philadelphia, PA 19104, USA*

Received April 14, 1990; revision accepted December 10, 1990

ABSTRACT

We have measured cosmic ray produced ($t_{1/2}$ = 1.5 million years) $^{10}$Be and ($t_{1/2}$ = 0.705 million years) $^{26}$Al in purified quartz fractions of selected rock samples from Antarctic mountains. From these data we calculate (1) mean erosion rates, for the limiting case of steady-state surface exposure to cosmic rays, and (2) minimum exposure ages, for the limiting case of no erosion. Calculated mean erosion rates are very low, on the order of a few times $10^{-5}$ cm/yr; we believe the sampling to be sufficient to generalize this result to exposed bedrock in Antarctica. In favorable cases it is possible to distinguish between the limiting cases: steady-state erosion seems a better description in such cases. Most samples, including some taken a few meters above the present ice level, seem to have been exposed for millions of years, without major episodes of burial or abrasion by ice.

## 1. Introduction

The surface of the earth is continuously undergoing changes as a result of weathering and erosion, plate tectonics and volcanic processes. Continental denudation with its complex rock–water interactions is the central process of global biogeochemical cycling of elements. Rates of denudation depend on a variety of factors, in particular rock properties and chemical composition, climate (especially rainfall), structure, and elevation. Thus they are quite variable on a regional scale. A primary step in most geomorphological studies is to gain understanding of the location-specific weathering and erosional processes, their rates and cycles over different time periods. It is known that the surface of the earth is changed not only by slow continuous erosion processes but also by drastic denudation events such as glaciation. A number of independent but mainly indirect methods have been used to determine rates of erosion [1–4].

The Antarctic continent is very different from the others. It has been covered with ice for millions of years, with only a few regions exposed to the elements. Of these features the most spectacular are the mountain ranges which project above the permanent ice sheet. These mountains, in particular the Trans-Antarctic mountains and the Yamato mountains, are impediments to the ice flow; hence they are responsible for the existence of neighboring "blue ice" regions where wind-induced ablation is more rapid than snow accumulation. These regions are interesting both in themselves and because thousands of meteorites have been collected from their surfaces [e.g., 5,6]. We and others have measured cosmic ray produced nuclides in both meteorites and ice and have used them to study the history of both [e.g.,7,8]. The present work is in some sense an extension of these studies.

Although the rates of production of these nuclides in terrestrial rocks are far lower than the corresponding rates in meteorites in space, or in the Earth's upper atmosphere, because of atmospheric shielding [9], the development of accelerator mass spectrometry (AMS) for radionuclides, and improvements in mass spectrometry for stable

0012-821X/91/$03.50 

rare gases, have made it possible in recent years to measure amounts of both radioactive and stable nuclides produced *in situ* in terrestrial samples [10–16].

These measurements have the potential to yield exposure times and erosion rates in terrestrial surface rocks [10,11,15,17,18]. The Antarctic mountains are appropriate for an early application of this new, direct technique of measurement.

Our work has concentrated on measuring $^{26}$Al and $^{10}$Be produced *in situ* in quartz. To apply this method, production rates and, in particular, the production ratio of these two nuclides must be well known. Recently, the values were experimentally determined in terrestrial quartz using glacially polished granite from the Sierra Nevada [19]. The production rate of $^{10}$Be was found to be 6.0 atom/g $SiO_2$ yr at sea level (geomagnetic latitude $> 50°$). The production rate of $^{26}$Al was determined to be 36.8 atom/g $SiO_2$ year, and the $^{26}$Al/$^{10}$Be ratio 6.1 [19]. The production rates increase with increasing altitude due to the decrease in atmospheric shielding. At 3 km altitude production is more than a factor of ten greater than at sea level. They also change with geomagnetic latitude due to the higher cut-off energy for cosmic ray primaries toward the equator. The production ratio of $^{26}$Al/$^{10}$Be is insensitive to these changes [19].

Both these production rates are extremely low. Fortunately the present detection limit for $^{10}$Be and $^{26}$Al by AMS is also quite low, about $10^6$ atoms. This allows meaningful measurements of $^{10}$Be and $^{26}$Al in 15 g of quartz exposed for 10,000 years at sea level, assuming an Al concentration of $< 100$ ppm in the quartz.

In this study, we apply the $^{26}$Al-$^{10}$Be method to study samples of exposed bedrock collected with appropriate geological controls from the Allan Hills, the Sör Rondane Mountains, the Tillite Glacier region, and the Wright Valley areas of Antarctica. Our purposes were: (1) to determine the range of erosion rates or (if they are very small) exposure times of rocks in these regions; (2) to assess, to the degree possible, the relative importance of fresh exposure events and steady-state erosion at these sites; and (3) in some cases, to determine whether important changes in the ice level have occurred there on a million-year time scale.

## 2. Sample description and experimental procedure

### *2.1. Geology of the samples*

Sampling areas are located on the Antarctic continent in Fig. 1. In addition to local and regional geologic data we must know altitude, latitude, longitude, the depth below the present surface, the slope of the local surface, and the fraction of "open" sky actually seen by the sample. This refers to surrounding mountains or outcrops which would shield the sample from cosmic ray bombardment [19]. Sample ID, latitude, longitude, and altitude are shown in Table 1. For this study, all samples were collected from flat horizontal bedrock surfaces unless noted and all of them experienced $2\pi$ bombardment (cosmic ray bombardment from the entire sky).

*Allan Hills region.* J. Schutt collected nine bedrock samples from the Allan Hills area and one from Reckling Peak during the 1985–86 field season for this study. Sample descriptions and distances from the present ice surface are given in Table 2. The sample locations are shown in Fig. 2. For comparison with the above samples, $^{10}$Be and $^{26}$Al were also measured in three loose rocks (ALH, ALHP, and MHB). The term loose rock is used to designate any non-bedrock sample such as pebbles, gravel, or moraine materials. Sample locations of these three rocks are also shown in Fig. 2. Sample RKP was cut into two portions, T (0–2.2 cm from the surface) and B (2.2–4.0 cm) for a reproducibility check. About 2000 meteorites have

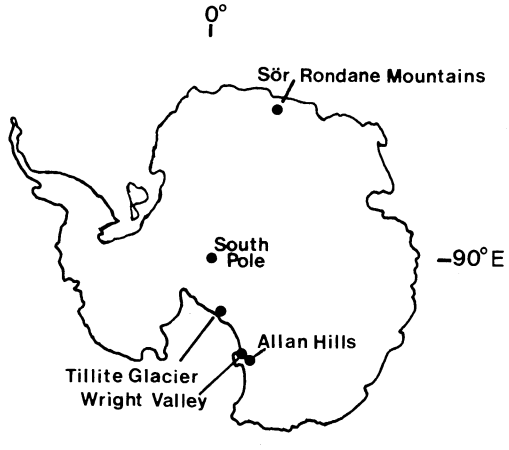


Fig. 1. Map of Antarctica showing sample locations.

TABLE 1

Sample location

| ID | Name | Latitude | Longitude | Altitude (m) |
|---|---|---|---|---|
| ALH85-1 | Allan Hills 85-1 | 76.7°S | 159.4°E | 2085 |
| ALH85-2 | Allan Hills 85-2 | 76.7°S | 159.4°E | 1955 |
| ALH85-3 | Allan Hills 85-3 | 76.7°S | 159.5°E | 2150 |
| ALH85-4 | Allan Hills 85-4 | 76.7°S | 159.6°E | 1807 |
| ALH85-5 | Allan Hills 85-5 | 76.7°S | 159.6°E | 1652 |
| ALH85-6 | Allan Hills 85-6 | 76.7°S | 159.6°E | 1625 |
| ALH85-7 | Allan Hills 85-7 | 76.7°S | 159.6°E | 1610 |
| ALH85-8 | Allan Hills 85-8 | 76.7°S | 159.6°E | 1615 |
| ALH85-9 | Allan Hills 85-9 | 76.7°S | 159.6°E | 1645 |
| RKP | Reckling Peak | 76.3°S | 159.3°E | 2010 |
| ALH * | ALH quartzite | 76.7°S | 159.6°E | 2050 |
| ALHP * | Allan Hills Peak | 76.7°S | 159.6°E | 2300 |
| MHB * | Manhaul Bay | 76.7°S | 159.6°E | 1600 |
| TAC-7 | Sör Rondane 860118-01 | 71.9°S | 25.2°E | 2120 |
| TAC-8 | Sör Rondane 860119-02 | 72.0°S | 25.2°E | 1410 |
| TAC-9 | Sör Rondane 860128-01B | 72.1°S | 26.2°E | 1410 |
| TAC-10 | Sör Rondane A860116-03-3 | 71.8°S | 25.7°E | 1180 |
| TAC-11 | Sör Rondane A860118-02B | 71.9°S | 25.4°E | 1470 |
| TAC-12 | Sör Rondane A860121-06B | 72.1°S | 25.1°E | 2650 |
| TAC-13 | Sör Rondane A860122-01 | 72.2°S | 25.2°E | 1700 |
| TAC-14 | Sör Rondane A860122-05C | 72.1°S | 25.1°E | 1800 |
| FM-A | Tillite Glacier FM-A | 83.9°S | 166.3°E | 2400 |
| FM-B * | Tillite Glacier FM-B | 83.9°S | 166.3°E | 2400 |
| BW85-80 | Wright Valley BW85-80 | 77.6°S | 161.1°E | 1850 |
| BW85-109 | Wright Valley BW85-109 | 77.6°S | 161.1°E | 1850 |
| BW85-114 | Wright Valley BW85-114 | 77.6°S | 161.3°E | 1900 |
| BW85-116 | Wright Valley BW85-116 | 77.6°S | 161.4°E | 1600 |

* Loose rocks

TABLE 2

Sample description of Allan Hills region

| ID | Above present ice (m) | Description |
|---|---|---|
| ALH85-1 | 15 | Quartz sandstone boulder in Mawson Formation from the highest point on a broad, flattish nunatak |
| ALH85-2 | 4 | Coarse grained quartz sandstone boulder in Mawson Formation; highest point on outcrop |
| ALH85-3 | 60 | Coarse grained quartz sandstone boulder in Mawson Formation; near highest point on broad flat top ridge |
| ALH85-4 | 8 | Coarse grained quartz sandstone boulder in Mawson Formation; top of small broad, flattish ridge; east of survey station #2. |
| ALH85-5 | | Beacon Sandstone outcrop; 300 m from ALH85-9 |
| ALH85-6 | | Beacon Sandstone outcrop; 580 m from ALH85-9 |
| ALH85-7 | | Beacon Sandstone outcrop; 915 m from ALH85-9 |
| ALH85-8 | | Beacon Sandstone outcrop. 1310 m from ALH85-9 |
| ALH85-9 | 0.2 | Beacon Sandstone outcrop; 1 m from present ice edge |
| ALH | | Loose rock; quarzite |
| ALHP | | Loose rock; near the peak of the Allan Hills; near the southern end of the range |
| MHB | | Loose rock from flat terrain just south of the Manhaul Bay ice tongue's greatest extent |
| RKP | 60 | Fractured sandstone xenolith in basalt on summit of Reckling Peak |

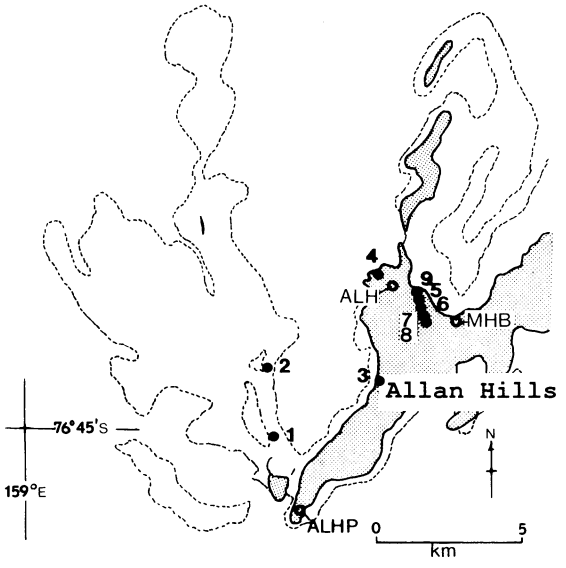


Fig. 2. Allan Hills, Allan Hills Icefield, and sample locations. Allan Hills 85 samples are indicated by a number and filled circle. Three loose rocks are shown as open circles.

been found in the Allan Hills Icefields which are located west of the Allan Hills. The terrestrial ages of these meteorites range from 2000 to 950,000 years [7].

*Sör Rondane Mountains.* A series of rock samples was collected for us by H. Kojima and K. Moriwaki from the Sör Rondane Mountains (72°S, 25°E) [20]. We selected eight of these samples (TAC 7-14) for the present study. The sampling locations are shown in Table 1 and Fig. 3. The Japanese expedition team found more than 2000 meteorites in this region in 1987–1989 [21]. Most of them were found on the Nansenisen blue ice which is located south of the Sör Rondane Mountains.

*Tillite Glacier area.* Two sandstone samples (FM-A and B) were collected for us from the top of a long ridge extending into the Tillite Glacier, Queen Alexandra Range by G. Faure in 1985. The Tillite Glacier flows into the Bowden Neve north of the Beardmore Glacier. This glacier is located about 70 km north east of Lewis Cliff where more than 2000 meteorites have been found. According to G. Faure, the sandstone beds exposed on the sampled ridge belong to the lower part of the Buckley Formation which is Permian in age. FM-A is indigenous bedrock and FM-B is a loose rock. The two sample locations are separated by ~ 500 m along the ridge top. Sample FM-B was cut into three portions, T (0–2.2 cm from the surface), M (2.2–4.4 cm), and B (4.4–6.5 cm).

*Wright Valley.* Four Beacon Supergroup sandstones were collected for us by R. Weed in 1986 from Asgard Range, which is on the south side of Upper Wright Valley, Dry Valley. The sampling locations are shown in Table 1. BW85-80 and 109 were collected from a horizontal sandstone platform on the Linnaeus Terrace, BW85-114 was collected from the platform dividing Cirque VI and VII, and BW85-116 was collected from the surface of another large flat platform.

### 2.2. *Chemical processing and AMS measurements*

The rock samples were ground to $< 700$ $\mu$m and quartz was separated by selective chemical dissolution [22]. The principal reasons for this purification were to reduce the Al content to a value where measurement of the $^{26}$Al/Al ratio was possible and to eliminate contamination from "garden variety" $^{10}$Be (i.e., that produced in the atmosphere). Be carrier (1.5 mg) was added to the purified quartz which was then dissolved with an HF-$HNO_3$ mixture. Al concentrations were measured by atomic absorption spectroscopy. The uncertainty in the Al measurement is 1.5–2% which is 3–4 times smaller than that for current AMS measurements. If the total amount of Al was less than 1 mg, appropriate amounts of Al carrier were added. Be and Al were separated and purified using anion exchange, acetylacetone solvent extraction, and cation exchange [23,24]. The $^{10}$Be and $^{26}$Al measurements were performed on the University of Pennsylvania's FN tandem Van de Graaff accelerator [25,26]. The measured $^{10}$Be/Be ratios ranged from $1 \times 10^{-12}$ to $2 \times 10^{-11}$ and the measured $^{26}$Al/Al ratios ranged from $1 \times 10^{-12}$ to $1 \times 10^{-10}$. These ratios are extremely high for terrestrial samples, even considering the large amounts of quartz (10–70 g) which were dissolved. Low-level standards, produced by dilution in La Jolla from the ICN (ICN Biomedical, Inc.) $^{10}$Be and NBS $^{26}$Al standards, were used for normalization. After making the background (due to $^{10}$B for $^{10}$Be measurements) and blank ($6 \times 10^{-15}$ for $^{10}$Be/Be and $1 \times 10^{-15}$ for $^{26}$Al/Al) corrections,

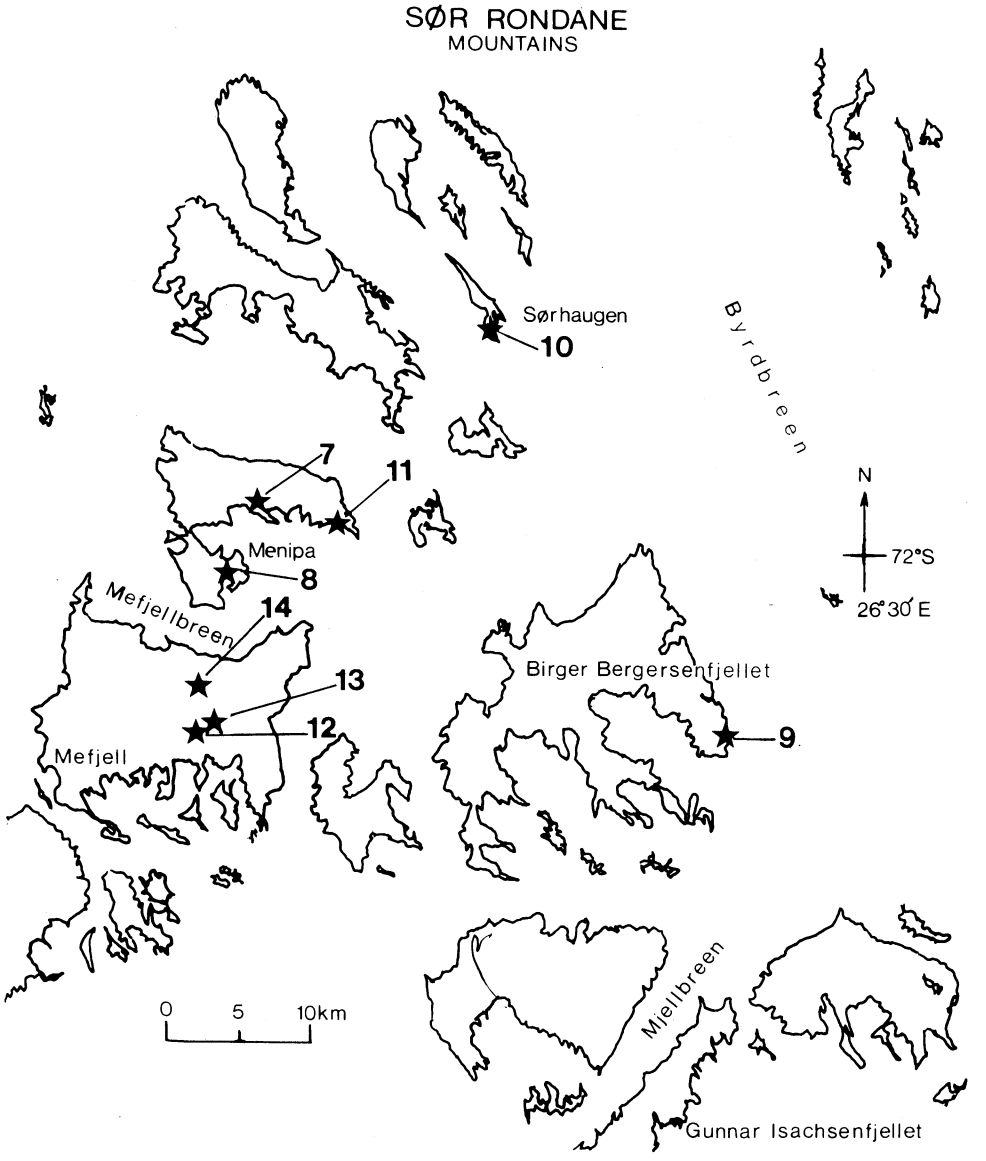


Fig. 3. Sör Rondane Mountains and sample locations of TAC-7–TAC-14.

the measured ratios were converted to atom concentrations (atom/g quartz).

## 3. Interpretation of *in situ* cosmogenic nuclide data and description of models

The physical basis of studying surficial processes with *in situ* produced nuclides is the attenuation of cosmic rays in traversing matter by nuclear interactions and ionization losses, which leads to a pronounced depth effect on the production rate of various nuclides. At depths in the atmosphere exceeding 200 g/cm$^2$ ($< 10$ km altitude) the nuclear cascade shows primarily an exponential attenuation, with little altitudinal variation in the energy spectrum of nuclear active particles, which are primarily neutrons and protons [27]. Consequently, the production rate of

nuclides can be taken to decrease exponentially with depth inside a target. For a flat horizontal target, the production rate of a cosmogenic nuclide, $P(x)$ (atom/g yr) varies with depth, $x$ (cm), according to the following equation:

$$P(x) = P(0)\, e^{-(\rho x/\Lambda)} \quad (1)$$

where $\rho$ is the mean density of the target rock (g/cm$^3$), $\Lambda$ is the absorption mean free path for nuclear interacting particles in the rock (g/cm$^2$), and $P(0)$ is the production rate of the cosmogenic nuclide at the rock surface. The interaction mean free path for $^{10}$Be and $^{26}$Al in rock on the surface of the earth has not yet been experimentally determined. In this paper we adopted a mean free path of 165 g/cm$^2$ for both nuclides. This value was estimated from measurements of the Apollo 15 lunar drill core (176 g/cm$^2$) [23,24] and from theoretical estimation (150 g/cm$^2$) [9]. Production by the capture of stopped muons and by reactions induced by fast muons becomes increasingly important with increasing depth in solid matter. The underground interaction mean free path for stopped muons is very different from that for neutron interactions [28,29]. However, nuclear interactions (spallation) create most of the activity measured in these studies since the samples are surface rocks with very low erosion rates (see below). The production rate, $P(0)$, increases with increasing altitude. It also increases with increasing geomagnetic latitude from 0 to 50° and then remains nearly constant above 50° [27,30]. Since all samples were collected from geomagnetic latitudes between 70 and 80°, the same sea level production rate, $P(0)$, can be applied to all of them. For complex target geometries such as angled surfaces or shielding by surrounding rocks, the cosmic ray attenuation has to be carefully calculated on a case by case basis as was done for the Sierra Nevada rocks [19].

The following is a brief discussion of the quantitative model; a more complete treatment can be found in [18]. The concentration of each nuclide increases with exposure time exactly as for extraterrestrial material but the interpretation of data is complicated by the erosion experienced by most terrestrial rocks. The nuclide concentration in most terrestrial samples is, in fact, controlled by the erosion rate [30]. For the simple case of a constant erosion rate, $\epsilon$ (cm/yr), the steady-state nuclide concentration in the rock surface, $N(0)$ (atom/g), is given by the following equation assuming a constant cosmic ray intensity:

$$N(0) = [P(0)]/[\lambda + (\rho\epsilon/\Lambda)] \quad (2)$$

Since the production rate, $P(0)$, the decay constant of the radionuclide, $\lambda$, the density of rock, $\rho$, and the absorption mean free path, $\Lambda$, are known, the erosion rate can be calculated from the nuclide concentration assuming continuous exposure. The same equation can be applied to the concentrations of *in situ* produced stable nuclides such as $^3$He and $^{21}$Ne with $\lambda$ taken to be 0. It is not necessary to consider continuous erosion on a microscale. If rock wastage occurs in steps of thickness small compared to $\Lambda$, we can average it to obtain a mean erosion rate $\epsilon$. It is only events removing material on a scale comparable to or greater than $\Lambda$ which can be considered individually, or in favorable cases dated.

However, nature is not always so simple, especially in Antarctica. There are many possible complex exposure scenarios. One likely history involves a thick ice sheet covering the rock and for a time effectively stopping cosmic ray production. Then glaciation suddenly erodes the old exposed surface. If we assume that the surface of the rock was exposed at some finite time $T$ years in the past with erosion rate, $\epsilon$, the radionuclide concentration is given by the following equation.

$$N(0) = [P(0)/(\lambda + \rho\epsilon/\Lambda)]\left[(1 - e^{-(\lambda+\rho\epsilon/\Lambda)T})\right] \quad (3)$$

Since equation (3) is controlled by $\epsilon$ and $T$, data on only one nuclide can lead to erroneous conclusions unless the erosion rate or the exposure age is known by some other determination. Using two or more radionuclides with different half-lives constrains the model. $^{26}$Al-$^{10}$Be in quartz is the ideal pair for many geological settings [17].

The $^{26}$Al/$^{10}$Be concentration ratio is plotted against $^{10}$Be content (atom/g quartz) in Fig. 4a. The $^{10}$Be content is normalized to sea level and geomagnetic latitude $> 50°$ [27]. The $^{26}$Al/$^{10}$Be ratio vs. $^{26}$Al content is plotted in Fig. 4b in analogy to Fig. 4a. The two solid curves on each figure represent the calculations for the two limiting cases discussed above: long-term steady-state erosion (lower curve), and sudden exposure at

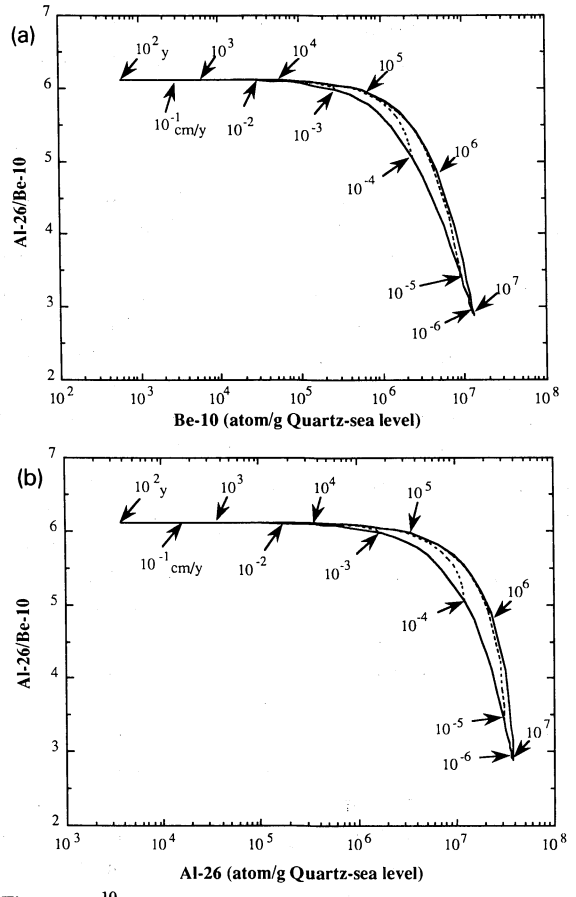


Fig. 4. (a) $^{10}$Be concentration (atom/g quartz at sea level) vs. $^{26}$Al/$^{10}$Be ratio. The upper curve is calculated for zero erosion with different exposure ages. The bottom curve is calculated for steady-state erosion. The erosion rates, $10^{-5}$, $10^{-4}$, and $10^{-3}$ cm/yr with finite exposure age are shown with dashed lines. Progress along the curve to the right represents increasing exposure time (upper curve) or decreasing erosion rate (lower curve) as indicated by the arrows. (b) $^{26}$Al concentration (atom/g quartz at sea level) vs. $^{26}$Al/$^{10}$Be ratio.

time $T$ with no subsequent erosion (upper curve). The $^{26}$Al/$^{10}$Be ratio with steady-state erosion, lower curve, is given by the equation:

$$\frac{^{26}\mathrm{Al}}{^{10}\mathrm{Be}} = \frac{N_{26}}{N_{10}} = \frac{P_{26}}{P_{10}} \frac{\lambda_{10} + \rho\epsilon/\Lambda}{\lambda_{26} + \rho\epsilon/\Lambda} \tag{4}$$

where $P_{26}/P_{10}$ is 6.10 at sea level ($> 50°$), the value obtained from the Sierra Nevada rocks [19]. $\lambda_{10}$ and $\lambda_{26}$ are the decay constants of $^{10}$Be and $^{26}$Al respectively. The $^{26}$Al/$^{10}$Be ratio is calculated to be constant at the value of the production ratio where $\lambda << \rho\epsilon/\Lambda$. This was the case for the samples from Meteor Crater [31]. The line continues as a smoothly varying function reaching an end point to the right at:

$$\frac{^{26}\mathrm{Al}}{^{10}\mathrm{Be}} = \frac{P26\ \lambda_{10}}{P_{10}\ \lambda 26} = 2.88 \tag{5}$$

which corresponds to the case of $\epsilon = 0$. The numbers given on the lower curve represent various erosion rates in cm/g.

The $^{26}$Al/$^{10}$Be ratio with finite exposure age is given as:

$$\frac{^{26}Al}{^{10}Be} = \frac{P_{26}\ \lambda_{10}}{P_{10}\ \lambda_{26}} \frac{1 - e^{-\lambda_{10}T}}{1 - e^{-\lambda_{26}T}} \tag{6}$$

The upper lines in Figs. 4a and b show this case. The numbers on these upper curves correspond to various exposure times in years with the termination of the curves at the lower right marking saturation in both nuclides. The cases of sudden exposure with subsequent erosion can be found in the window between the two lines. Curves for erosion rates of, $10^{-5}$, $10^{-4}$, and $10^{-3}$ cm/yr with finite exposure ages are shown in Figs. 4a and b as dashed lines.

Any rock surface undergoing steady or episodic erosion will have $^{26}$Al and $^{10}$Be concentrations, and a ratio $^{26}$Al /$^{10}$Be, falling in the zone bounded by the upper curve (single event) and the lower curve (steady-state) in Figs. 4a and b, if the conditions of the model hold. Points below or to the left of the lower curve imply significant episodes of burial by soil, snow, or ice. Points in the region above and to the right of the permitted zone can only be explained by some anomalous source of excess radionuclide concentration (for example, if the sample had actually been exposed to cosmic rays at a higher altitude than it was found, if there was another source of radiation in the surrounding environment, or if all "garden variety" activity was not removed during processing) or by experimental error.

## 4. Results and discussion

The $^{10}$Be and $^{26}$Al concentrations measured in quartz extracted from various Antarctic rock samples are given in Table 3. The Al concentrations in the purified quartz are also shown in the table. The $^{10}$Be and $^{26}$Al concentrations in the ALH samples have been previously reported [10]. The

ALH values given here include a 6.7% change in the $^{10}$Be results due to adoption of a different half-life for the nuclide (1.5 million years compared to the previous value of 1.6 million years). Table 4 lists exposure ages assuming zero erosion and steady-state erosion rates assuming constant exposure calculated for each sample using measured $^{10}$Be and $^{26}$Al concentrations and equations (3 with $\epsilon = 0$) and (2), respectively. The data were corrected for altitude effects before calculation. If the sample was exposed to cosmic rays without a special history, such as burial or coverage by a thick ice sheet, then the exposure age in the table indicates a minimum exposure time, since the calculation assumes no erosion, and the erosion rate in the table represents a maximum erosion rate. All calculations are based on the production rates of $^{10}$Be and $^{26}$Al obtained from Sierra Nevada rocks [19]. The errors for the calculated exposure ages (Table 4) do not include an error of approximately 10% for the production rate used to obtain them. This production rate uncertainty comes primarily from the uncertainty in the time of deglaciation of the polished Sierra Nevada rocks. Applying these [19] experimentally obtained production rates to other locations may involve small additional errors due to altitude and geomagnetic latitude corrections. We expect these errors to be minor in the present study. Although the altitude correction from the sampling location to sea level contributes a small error ($<$ a few%) due to uncertainties in the attenuation length for nuclear interactions and stopped muons in the atmosphere, the altitude of the Sierra Nevada rocks and the Antarctic rocks studied here are very similar and any error in the altitude correc-

TABLE 3

Results of $^{10}$Be and $^{26}$Al in Antarctic rocks

| ID | Weight (g) | Al content (ppm) | $^{10}$Be ($10^6$ atom/g $SiO_2$) | $^{26}$Al ($10^6$ atom/g $SiO_2$) | $^{26}$Al/$^{10}$Be |
|---|---|---|---|---|---|
| ALH85-1 | 20.85 | 128 | 37.21 ± 2.31 | 135.1 ± 6.1 | 3.63 ± 0.28 |
| ALH85-2 | 15.15 | 169 | 10.72 ± 0.72 | 51.77 ± 2.76 | 4.83 ± 0.42 |
| ALH85-3 | 20.06 | 128 | 26.27 ± 1.92 | 102.3 ± 4.6 | 3.90 ± 0.33 |
| ALH85-4 | 34.90 | 63 | 26.61 ± 1.34 | 99.42 ± 4.37 | 3.74 ± 0 25 |
| ALH85-5 | 20.07 | 101 | 18.63 ± 1.14 | 73.43 ± 3.48 | 3.94 ± 0.31 |
| ALH85-6 | 16.53 | 350 | 14.49 ± 0.90 | 56.34 ± 3.13 | 3.89 ± 0.32 |
| ALH85-7 | 15.56 | 301 | 12.71 ± 0.88 | 54.04 ± 3.16 | 4.25 ± 0.39 |
| ALH85-8 | 10.31 | 390 | 11.35 ± 0.73 | 56.36 ± 3.31 | 4.97 ± 0.43 |
| ALH85-9 | 17.24 | 405 | 16.13 ± 1.00 | 63.99 ± 3.01 | 3.97 ± 0.31 |
| RKP-T | 19.92 | 781 | 5.95 ± 0.40 | 32.84 ± 2.65 | 5.52 ± 0.58 |
| RKP-B | 20.91 | 872 | 6.11 ± 0.39 | 33.72 ± 2.06 | 5.52 ± 0.49 |
| ALH | 13.09 | 467 | 42.75 ± 1.71 | 201.1 ± 19.8 | 4.70 ± 0.50 |
| ALHP | 11.16 | 70 | 30.15 ± 2.15 | 55.67 ± 3.91 | 1.85 ± 0.19 |
| MHB | 10.42 | 20 | 15.62 ± 1.88 | 55.04 ± 4.88 | 3.53 ± 0.53 |
| TAC-7 | 26.06 | 32 | 34.47 ± 0.86 | 132.7 ± 8.0 | 3.85 ± 0.25 |
| TAC-8 | 41.29 | 54 | 3.14 ± 0.09 | 16.11 ± 0.66 | 5.13 ± 0.26 |
| TAC-9 | 31.43 | 34 | 0.844 ± 0.030 | 3.46 ± 0.25 | 4.09 ± 0.33 |
| TAC-10 | 20.98 | 18 | 20.94 ± 0.61 | 82.08 ± 4.13 | 3.92 ± 0.23 |
| TAC-11 | 42.42 | 47 | 15.77 ± 0.60 | 70.69 ± 2.68 | 4.48 ± 0.24 |
| TAC-12 | 16.12 | 31 | 80.27 ± 1.93 | 270.3 ± 13.6 | 3.37 ± 0.19 |
| TAC-13 | 30.50 | 22 | 42.76 ± 1.07 | 136.1 ± 5.1 | 3.18 ± 0.14 |
| TAC-14 | 36.81 | 14 | 58.06 ± 1.34 | 168.7 ± 6.6 | 2.91 ± 0.13 |
| FM-A | 30.21 | 135 | 43.30 ± 2.64 | 189.8 ± 9.5 | 4.38 ± 0.35 |
| FM-B-T | 29.95 | 106 | 64.98 ± 4.03 | 272.6 ± 16.3 | 4.20 ± 0.36 |
| FM-B-M | 30.31 | 110 | 61.63 ± 3.75 | 268.3 ± 16.2 | 4.35 ± 0.37 |
| FM-B-B | 30.59 | 111 | 64.27 ± 3.91 | 247.7 ± 15.0 | 3.85 ± 0.33 |
| BW85-80 | 30.87 | 83 | 11.42 ± 0.70 | 61.89 ± 3.09 | 5.42 ± 0.43 |
| BW85-109 | 25.66 | 66 | 18.20 ± 1.12 | 87.44 ± 4.48 | 4.80 ± 0.39 |
| BW85-114 | 65.39 | 74 | 9.69 ± 0.59 | 52.60 ± 2.60 | 5.43 ± 0.47 |
| BW85-116 | 71.74 | 76 | 10.20 ± 0.62 | 57.86 ± 4.06 | 5.68 ± 0.53 |

TABLE 4

Exposure age and erosion rate of Antarctic rocks

| ID | Minimum exposure age ($10^3$ yr) | Maximum erosion rate (m/$10^6$ yr) |
|---|---|---|
| ALH85-1 | 1400±340 | 0.24±0.02 |
| ALH85-2 | 370± 40 | 1.31±0.07 |
| ALH85-3 | 830±190 | 0.51±0.07 |
| ALH85-4 | 1150±270 | 0.32±0.04 |
| ALH85-5 | 700±160 | 0.63±0.10 |
| ALH85-6 | 620±160 | 0.73±0.14 |
| ALH85-7 | 560±100 | 0.81±0.10 |
| ALH85-8 | 530± 30 | 0.85±0.05 |
| ALH85-9 | 850±190 | 0.49±0.06 |
| RKP | 200± 10 | 2.53±0.10 |
| ALH | 2100±140 | 0.07±0.12 |
| ALHP | 600±500 | 1.1 ±0.9 |
| MHB | 660±220 | 0.70±0.21 |
| TAC-7 | 1240±240 | 0.28±0.01 |
| TAC-8 | 150± 20 | 3.39±0.24 |
| TAC-9 | 36± 10 | 15.6 ±4.2 |
| TAC-10 | 1770±170 | 0.17±0.04 |
| TAC-11 | 880± 80 | 0.45±0.02 |
| TAC-12 | 3000±400 | 0.05±0.02 |
| TAC-13 | 2900±800 | 0.06±0.01 |
| TAC-14 | > 4000 | < 0.06 |
| FM-A | 1500±110 | 0.21±0.07 |
| FM-B | 3000±410 | < 0.11 |
| BW85-80 | 460± 20 | 1.00±0.10 |
| BW85-109 | 770± 40 | 0.54±0.05 |
| BW85-114 | 370± 20 | 1.31±0.08 |
| BW85-116 | 520± 30 | 0.88±0.15 |

tion should therefore nearly cancel out. Since the geomagnetic latitude of the Sierra Nevada rocks, 44°, is close to the region 50–90° where the geomagnetic correction is unity, this correction is relatively small, only 14% at 2000 m altitude. The production ratio $^{26}Al/^{10}Be$ should be free of these errors and known accurately. The detailed correction methods and parameters are given elsewhere [19,27]. Results from one Sör Rondane sample, TAC-14, give exactly the calculated saturation value for both the nuclides increasing our confidence in these production rates (see below).

The outstanding features of Table 4 are the long exposure ages and correspondingly low erosion rates for many of the samples. More than 1/3 of the samples have exposure ages over 1 million years and most of the samples have erosion rates of only a few $\times 10^{-5}$ cm/year or less. Calculations made separately for the two nuclides are in agreement although saturation of $^{26}Al$ limits the accuracy of comparison in many cases. These ages and erosion rates are in marked contrast to results from other continents. Erosion rates for rocks from more temperate continents have been found to be generally in the range $10^{-2}$–$10^{-4}$ cm/yr [1–4,10]; rocks from such locations would never develop the high (saturated) concentrations of $^{10}Be$ and $^{26}Al$ seen in Antarctica. The samples from each site area are discussed separately in the following sections.

### 4.1. *Allan Hills*

The $^{26}Al/^{10}Be$ ratios vs. the $^{10}Be$ concentrations (atom/g quartz at sea level) for nine ALH85 and RKP samples are shown in Fig. 5 by filled squares. Three loose rock samples, ALH, ALHP, and MHB, are shown in the figure as open circles. The experimental error of the $^{10}Be$ measurements are within the symbols. The graph of $^{26}Al/^{10}Be$ ratio vs. $^{26}Al$ concentration (atom/g quartz at sea level) for these samples (not shown) is similar to Fig. 5.

The surface ice movements at the Allan Hills Main Icefield have been investigated using a triangulation network over the last 10 years [32,33]. In general the ice moves from south to north and the velocity decreases to a few cm/yr on the northeast end of the Main Icefield (near the Allan Hills). A radio echo sounding survey has mapped

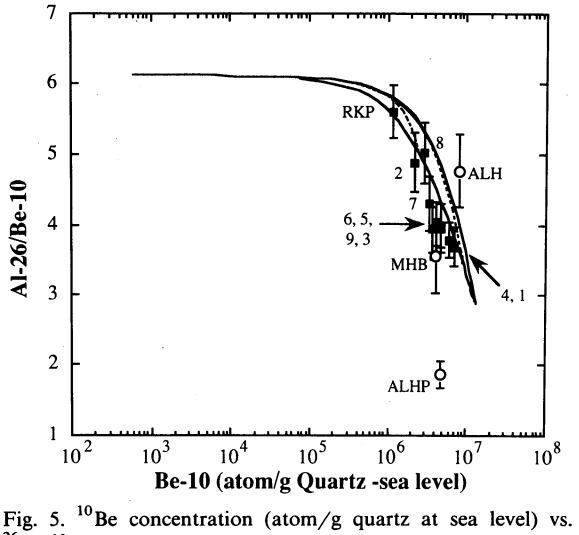


Fig. 5. $^{10}Be$ concentration (atom/g quartz at sea level) vs. $^{26}Al/^{10}Be$ ratio for samples collected from the Allan Hills region. ALH-85 and RKP samples are shown with filled squares and ID number. Three loose rocks are shown with open circles.

the subice topography of the Allan Hills Main Icefield and the Near Western Icefield [34]. The Allan Hills Main Icefield covers an area of relatively shallow bedrock (mesa) which is separated by a deep valley from the Near Western Icefield [34]. The area containing the high meteorite concentration corresponds closely to the area of relatively shallow bedrock. ALH85-1 and ALH85-2 were taken from outcrops of this mesa. Since the current ice surface is very close to many of the locations sampled (Table 2), long steady-state cosmic ray exposure was not expected for this series of samples. The calculated minimum exposure ages and maximum erosion rates for these samples are shown in Table 4. The data indicate that the Allan Hills have been exposed above the present ice surface for more than a half-million years and that the erosion rate for these rocks is less than a few times $10^{-5}$ cm/yr. The major question is whether the Allan Hills were continuously exposed for the more than half-million year time period or whether a thick ice sheet overflowed the area within the past few 100,000 years.

The $^{26}$Al/$^{10}$Be-$^{10}$Be concentration diagram (Fig. 5) shows that all ALH85 samples are on the steady-state erosion line or slightly to the left of the line. The samples which do not fall on the erosion line can be explained by past partial ice or snow cover. The outcrop sample ALH85-1 contains the highest $^{10}$Be and $^{26}$Al concentrations of any of these samples and falls on the erosion line. This boulder was exposed above the ice surface for more than 1.4 million years and experienced an erosion rate of less than $2.5 \times 10^{-5}$ cm/yr. Three meteorites were found on soil at this outcrop. Their terrestrial ages should provide useful comparison to the exposure time of the surface rock.

Samples ALH85-5 to ALH85-9 were collected along a 1.3 km transect next to Manhaul Bay (an icefield located north of the Allan Hills). ALH85-9 was collected 1 m from the edge of the ice and 20 cm above the existing ice surface. Since all samples were taken near the ice surface and from almost the same elevation, we expected them to show evidence for similar ice cover histories. ALH85-5, 6, 7, and 9 plot in a similar region in Fig. 5; somewhat shifted toward the left from the erosion line. This indicates that the sample location was exposed above the ice surface for more than 0.6 million years and experienced at least one episode of burial during the exposure history.

Reckling Peak is located about 50 km north of Allan Hills. The Reckling Peak sample (RKP) shows the highest erosion rate, $2.7 \times 10^{-4}$ cm/yr, of all the Antarctic rocks studied in this work. The peak has been exposed above the glacier for more than 0.2 million years.

*4.2. Sör Rondane*

The $^{26}$Al/$^{10}$Be ratios vs. the $^{10}$Be concentrations (atom/g quartz at sea level) for the Sör Rondane Mountain samples are shown in Fig. 6. Some conclusions can be drawn about the individual sampling sites although in several cases there are more samples to be measured. TAC-7 is from near the peak of Menipa Mountain 650 m higher than the Mefjellbreen. Field observations show well oxidized surfaces for this bedrock indicative of long exposure. The results in Fig. 6 and Table 4 indicate a continuous exposure of over 1 million years for this sample. The erosion rate for this sample is quite low. TAC-8 is from the opposite side of the local glacier; it was taken from the southeast facing slope of Menipa, ~ 150 m higher than the Mefjellbreen. The low $^{26}$Al/$^{10}$Be ratio for this sample compared to its concentration of $^{10}$Be (position on Fig. 6 to the left of the calculated curves) indicates a complex history and is consistent with the location sampled which is closer to

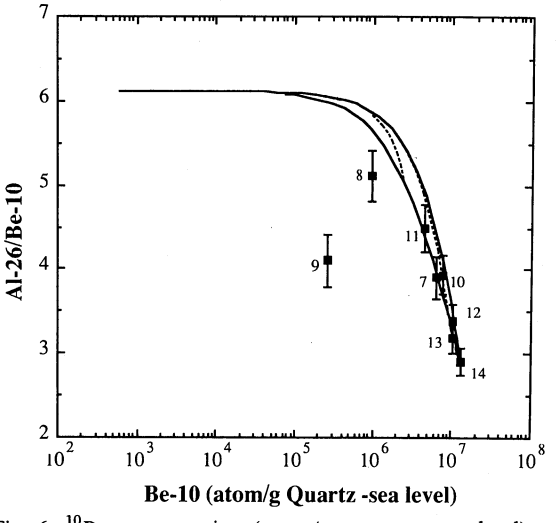


Fig. 6. $^{10}$Be concentration (atom/g quartz at sea level) vs. $^{26}$Al/$^{10}$Be ratio for Sör Rondane samples. TAC-numbers are indicated.

the ice surface. TAC-9 was taken from the south side of the east wall of Birger Bergersenfjellet 3 m above the surface of the Byrdbreen ice sheet. The 36,000 year exposure age measured for this sample is short compared to other samples in the area, as expected. The low $^{26}Al/^{10}Be$ ratio compared to its $^{10}Be$ concentration must be due to a complex history of exposure and reburial in the ice. This is clear from its distance to the left of the curves on Fig. 6. TAC-10 is from the east slope of Sörhaugen. It was taken from a pegmatite dike cutting approximately vertically through the rock mass. A series of five samples were taken from different altitudes; we report here on the one taken 25 m down from the highest location sampled. Continuous exposure over the last 1 million years or more with a low erosion rate of $1.7 \times 10^{-5}$ cm/yr is indicated for this sample. TAC-11 was collected from near the peak of the local rock mass. Elevation is 450 m higher than the Mfjellbreen but the $^{26}Al/^{10}Be$ ratio indicates a simple exposure history with a $4.8 \times 10^{-5}$ cm/yr erosion rate.

TAC-12, 13, and 14 are from the crests of the highest ridges on Mefjell Mountain. The samples differ in altitude by nearly 950 m and the lowest sample is at least a few hundred meters higher than the present ice surface. These samples are nearly saturated in $^{10}Be$, implying a long exposure with little ($< 10^{-5}$cm/yr) erosion. The minimum exposure ages are 2.9 to 4.0 million years. $^{26}Al$ is nearly saturated in these samples as is shown by the $^{26}Al/^{10}Be$ ratio of $\sim 3$. Clearly, this mountain mass has not been covered by ice for any significant period of time within the last 3 million years. One significant feature of Fig. 6 is that the measurements for TAC-14 fall at the end point of the curves indicating saturation for both nuclides. This agreement with the saturation production calculated using the rocks from the Sierra Nevada is discussed in a later section. In general the presently exposed mountains in the Sör Rondane area have been ice free for at least 1 million years, and the ice thickness has not been substantially greater than it is at present. The erosion rates for all these samples are very similar, suggestive of a common erosion mechanism, with no dependence on the direction the surface faces.

Over 2000 meteorites have been collected near the Sör Rondane Mountains [21] but samples have not yet been received for study. We intend to measure terrestrial ages for these objects which will help define the history of the ice in this region of Antarctica as has been done for the Allan Hills. Given the exposure ages of the Sör Rondane terrestrial rocks and the evidence for a constant ice level, these meteorites may have been accumulating for a long time and may show long terrestrial ages.

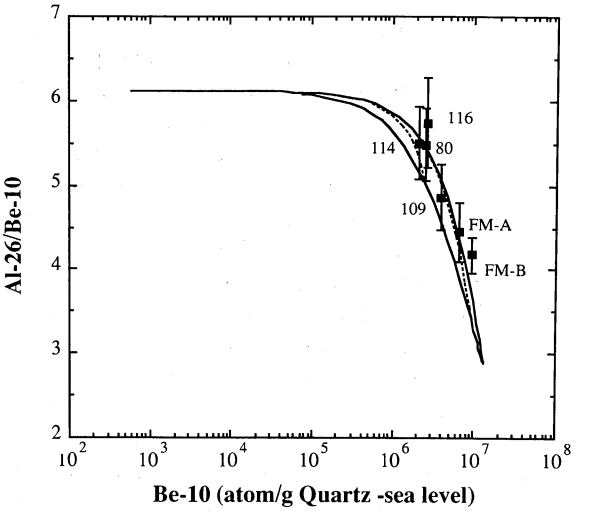


Fig. 7. $^{10}Be$ concentration (atom/g quartz at sea level) vs. $^{26}Al/^{10}Be$ ratio for Tillite Glacier (FM) and Wright Valley samples (BW).

*4.3. Tillite Glacier*

The sample FM-A falls on the exposure curve in Fig. 7; indicating an exposure of over 1.5 million years. On the other hand, the loose rock FM-B presents the problem of falling to the right of the curves in Fig. 7, in the forbidden region. The best explanation at the present time for FM-B is that this sample was exposed to cosmic rays at a higher altitude than where the sample was collected. The observed concentrations of $^{10}Be$ and $^{26}Al$ in FM-B correspond to the production at 2800 m or higher altitude. The sample was collected several km down slope from Mt. MacKellar (4297 m). FM-B may have been transported from the slope of Mt. MacKellar by ice movement in the past. The high activities of both nuclides in the FM samples are inconsistent with the fairly recent deglaciation that has been suggested for this site.

*4.4. Wright Valley*

The samples collected at Wright Valley, the BW-85 series samples, have a $^{26}Al$-$^{10}Be$ pattern

which is most easily interpreted as undersaturation. These rocks have been recently exposed with a minimum exposure age of approximately 0.5 million years. Their erosion rates are low, similar to rocks from other areas in Antarctica. The errors are large which makes further interpretation difficult; however all data points on Fig. 7 do overlap the erosion region.

A relatively short exposure for these samples is consistent with their lack of the silicious surface weathering features usually seen on surfaces in this region of Antarctica [R. Weed, pers. commun.]. The Transantarctic Mountains have been overridden by ice at various times [35]. The most recent direct glacial influence on the location sampled for this study has been tentatively dated at 0.3–0.5 million years ago [36] in agreement with the exposure ages measured here.

## 5. Verification of production rates for $^{10}$Be and $^{26}$Al

Figure 8a is an expansion of Fig. 6 with a linear-linear scale, showing the saturation end point of the calculated curves. Here again the lower line represents constant steady-state erosion and the upper line corresponds to sudden exposure with no subsequent erosion. Figure 8b is the same graph with $^{26}$Al on the $x$ axis. The altitude corrected values measured for TAC-14 for $^{10}$Be, $^{26}$Al, and the ratio, overlap the calculated end point of the curves within ~ 2%, well within the 1s uncertainty. This verifies the production rates of $^{10}$Be and $^{26}$Al obtained from the Sierra Nevada samples, [19] as well as substantiating the method used for altitude corrections. Our confidence in this conclusion is increased by the other TAC samples which overlap the steady-state erosion line within their 1s error and which also lie close to the end point of the two curves.

TAC-7, -11, -12, and -13 all overlap the steady-state erosion line but not the line for sudden exposure with zero erosion. TAC-10 falls in the window between the two cases on the finite exposure $10^{-5}$ cm/yr erosion line. TAC-12 falls in the window at a smaller erosion rate. The exposure history of TAC-10 can be calculated based on equation (3). The results (with a large error) is that TAC-10 was exposed to cosmic rays for 2.7 million years with $1 \times 10^{-5}$ cm/yr erosion rate.

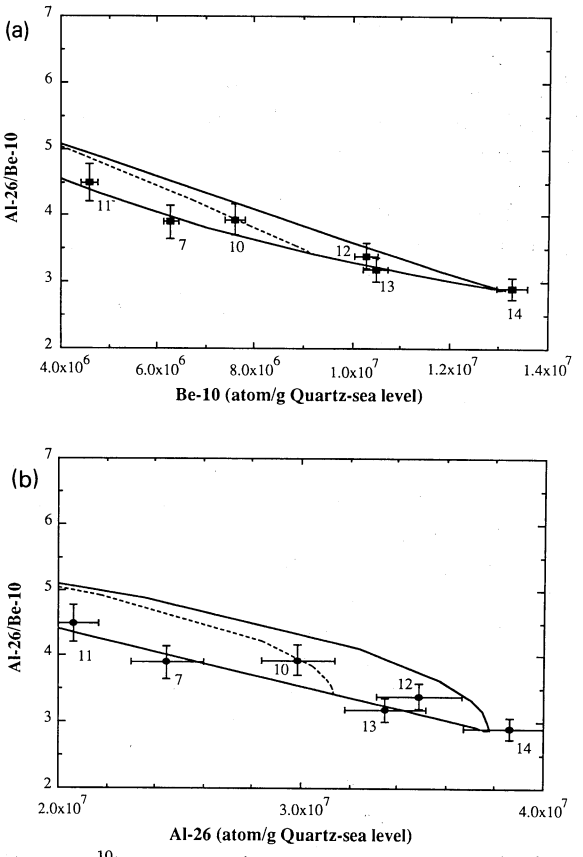


Fig. 8. (a) $^{10}$Be concentration (atoms/g quartz at sea level) vs. $^{26}$Al/$^{10}$Be ratio (linear scale). This is an expansion of a portion of Fig. 6. TAC numbers are indicated for Sör Rondane samples. The dashed line represents a finite exposure with an erosion rate of $10^{-5}$ cm/yr. (b) $^{26}$Al concentration (atoms/g quartz at sea level) vs. $^{26}$Al/$^{10}$Be ratio (linear scale). TAC numbers are indicated for Sör Rondane samples. The dashed line represents a finite exposure with an erosion rate of $10^{-5}$ cm/yr.

More precise measurements by AMS would allow us to define the combination of exposure age and erosion rate within reasonable limits. This means that measurement of only one nuclide would give an erroneous exposure age but that with both $^{10}$Be and $^{26}$Al it is possible, in favorable cases, to determine the exposure age and erosion rate.

The absolute positions of points in Fig. 8 (and earlier figures) depend on calibration data determined in [19]. For geomagnetic latitudes above 50° no latitude corrections are needed; for the Sierra Nevada rocks used there may be small but significant uncertainties both in the proper mean geomagnetic latitude over the period of the ex-

posure and in the length of the exposure period as derived from $^{14}C$ dates. The production ratio $^{26}Al/^{10}Be$ is of course well fixed and almost independent of latitude and altitude. Using this ratio, a steady-state concentration ratio of 2.9 is defined. Given this, Fig. 8 demonstrates that the calibration derived in [19] is valid at high latitudes within 10%, which seems the maximum lateral shift in these curves that can be tolerated. This does not rule out the possibility of needed corrections at lower latitudes, because of compensating errors.

## 6. Conclusions

Few studies have considered erosion rates in the Antarctic mountain ranges. Campbell and Claridge [37] have undertaken a primarily qualitative study of erosion and landform evolution in Antarctica. They find consistent evidence of stable surfaces with correspondingly low erosion rates, but do not give quantitative values. The results reported here provide the first quantitative information available on long-term erosion history. Malin [38] conducted a field study where he exposed various rock targets to the prevailing weather in the Dry Valley and Allan Hills areas. He measured weight loss of exposed rocks and converted to erosion rates (a few mg/cm$^2$ year).His results indicate erosion rates of $10^{-2}$–$10^{-3}$ cm/yr over the short (1 year) time scale of the experiment. These results are a few orders of magnitude lower than wind tunnel experiments [39] used to investigate formation of ventifacts in Antarctic rocks. In contrast to Malin we found erosion rates of $10^{-5}$ cm/yr or less on time scales of 105–106 years. The difference may be due to variability of weather conditions (a year vs. millions of years), or to experimental difficulties with the short-term experiments. Meteorites in the Allan Hills area with intact fusion crusts ~ 1 mm thick have terrestrial ages typically 104–105 years. The erosion rates for these objects (assuming long exposure on the surface, not just long terrestrial age) must be less than $10^{-5}$ cm/yr.

The information available from the *in situ* cosmic ray produced $^{10}Be$-$^{26}Al$ pair, at present levels of precision, is in general not quite sufficient to decide between the two limiting models illustrated in Figs. 4–8. Given the complexities of real geologic histories, however, one can hope only for a good approximation to one or the other, in most cases. It is important here to point out the importance of accurate knowledge of the ratio $^{26}Al/^{10}Be$. Measurement of one nuclide alone gives much less definitive information on the exposure history.

Except for the two Sör Rondane samples discussed above, there is no evidence among our samples for extensive burial periods between exposures, or for increased thickness of the ice sheet on a time scale of a million years. A significant fraction of the samples, with $^{26}Al/^{10}Be$ ratios not far from 3, can be considered to have been first exposed at least 3 million years ago, and perhaps much earlier. Measurement of $^{21}Ne$ or another stable nuclide would be valuable in defining the early history. For the others, whose $^{26}Al/^{10}Be$ ratios are significantly greater, we can only give a minimum period of exposure (Table 4) on the probably unrealistic assumption of zero erosion. For any sample with $^{26}Al/^{10}Be$ significantly less than 6, a stable noble gas measurement would be the best step to defining a true date of first exposure. At present we believe it likely that for many of these the limit of steady erosion, and early exposure, will prove to be more correct. This is suggested both by the geological evidence and the position of the points in Figs. 4–8. Studies of *in situ* produced $^{14}C$, $^{3}He$, and $^{21}Ne$ which are underway in these samples should help us resolve this question.

Additional samples from a variety of sites in Antarctica are necessary for unravelling specific geologic questions. This need has been discussed in the previous section for the Sör Rondane area. The Yamato mountains are another region which needs further study. Exposure age/erosion rate determinations of well selected rock samples from this area could be combined with existing meteorite data to clarify the local history of the ice and define specific meteorite accumulation mechanisms.

Except for areas of active moraine development, to be discussed elsewhere, we have seen no evidence of rapid erosion in Antarctica.

Very old surfaces with corresponding low erosion rates, have been thought to occur on other continents [40]. However, no other continent seems likely to show the extremely low erosion rates seen in these suites of samples from widely separated

locations in Antarctica. The absence of significant liquid water flows or frost-shattering has given this continent a unique history, at least since the development of a continent-wide ice sheet.

## Acknowledgements

The authors wish to thank W. Cassidy, G. Faure, H. Kojima, K. Moriwaki, S.A. Sandford, J. Schutt, and R. Weed for providing well documented and characterized samples. We also thank G. Faure, H. Kojima, D. Lal, and K. Moriwaki for many useful discussions and F. Shapiro for sample preparation. This work was initially supported by NASA Grant NAG 9-33. A part of this work was supported by NSF Grant ERA 86-17994.

## References

1 S. Judson, Erosion of the land, or What's happening to our continents? Am. Sci. 56, 356–374, 1968.
2 J.D. Milliman and R.H. Mead, World-wide delivery of river sediment to the oceans, J. Geol. 91, 1–21, 1983.
3 I. Saunders and A. Young, Rates of surface processes on slopes, slope retreat and denudation, Earth Surf. Process. Landforms 8, 473–501, 1983.
4 P. Pinet and M. Sourian, Continental erosion and large-scale relief, Tectonics 7, 563–582, 1988.
5 K. Yanai, Yamato-74 meteorites collection; Antarctica from November to 1974, Mem. Natl. Inst. Polar Res., Spec. Issue 8, 1–37, 1978.
6 I.M. Whillans and W.A. Cassidy, Catch a falling star: Meteorites and old ice, Science 222, 55–57, 1983.
7 K. Nishiizumi, D. Elmore and P.W. Kubik, Update on terrestrial ages of Antarctic meteorites, Earth Planet. Sci. Lett. 93, 299–313, 1989.
8 K. Nishiizumi, A.J.T. Jull, G. Bonani, M. Suter, W. Wölfli, D. Elmore, P.W. Kubik and J.R. Arnold, Age of Allan Hills 82102, a meteorite found inside the ice, Nature 340, 550–552, 1989.
9 D. Lal, In situ produced cosmogenic isotopes in terrestrial rocks, Ann. Rev. Earth Planet. Sci., 16, 355–388, 1988.
10 K. Nishiizumi, D. Lal, J. Klein, R. Middleton and J.R. Arnold, Production of $^{10}$Be and $^{26}$Al by cosmic rays in terrestrial quartz *in situ* and implications for erosion rates, Nature 319, 134–136, 1986.
11 F.M. Phillips, B.D. Leavy, N.O. Jannik, D. Elmore and P.W. Kubik, The accumulation of cosmogenic chlorine-36 in rock: a method for surface exposure dating, Science 231, 41–43, 1986.
12 H. Craig and R.J. Poreda, Cosmogenic $^{3}$He in terrestrial rocks: The summit lavas of Maui, Proc. Natl. Acad. Sci. U.S.A. 83, 1970–1974, 1986.
13 M.D. Kurz, Cosmogenic helium in a terrestrial igneous rock, Nature 320, 435–439, 1986.
14 J. Klein, R. Giegengack, R. Middleton and P. Sharma, Revealing histories of exposure using *in situ* produced $^{26}$Al and $^{10}$Be in Lybian desert glass, Radiocarbon 28, 547–555, 1986.
15 K. Marti and H. Craig, Cosmic-ray-produced neon and helium in the summit lavas of Maui, Nature 325, 335–337,1987.
16 A.J.T. Jull, D.J. Donahue, T.W. Linick and G.C. Wilson, Spallogenic $^{14}$C in high-altitude rocks and in Antarctic meteorites, Radiocarbon 32, 1990.
17 D. Lal and J.R. Arnold, Tracing quartz through the environment, Proc. Indian Acad. Sci. (Earth Planet. Sci.) 94, 1–5, 1985.
18 D. Lal, Cosmic ray labeling of erosion surfaces: *in situ* production rates and erosion models, Earth Planet. Sci. Lett. 104, 424–439, this issue, 1991.
19 K. Nishiizumi, E.L. Winterer, C.P. Kohl, J. Klein, R. Middleton, D. Lal and J.R. Arnold, Cosmic ray production rates of $^{10}$Be and $^{26}$Al in quartz from glacially polished rocks, J. Geophys. Res. 94, 17907–17915, 1989
20 K. Moriwaki, H. Kojima, H. Ishizuka, N. Matsuoka, T. Kometani, S. Shiga, T. Morita and S. Kuriki, Report on the geological, geomorphological and geodetic field party in the Sör Rondane Mountains, 1986 (JARE-27), Nankyoku Shiryo (Antarctic Record), 31, 246–281, 1986.
21 K. Yanai and the JARE-29 Asuka Party, The meteorite concentration of the bare ice surface around the Sör Rondane Mountains, Antarctica, 14th Symposium on Antarctic Meteorites, (Natl. Inst. Polar Res. Tokyo), 1, 1989.
22 C.P. Kohl and K. Nishiizumi, Isolation of quartz for $^{10}$Be and $^{26}$Al determination, in prep., 1990
23 K. Nishiizumi, D. Elmore, X.Z. Ma and J.R. Arnold, $^{10}$Be and $^{36}$Cl depth profiles in an Apollo 15 drill core, Earth Planet. Sci. Lett. 70, 157–163, 1984a.
24 K. Nishiizumi, J. Klein, R. Middleton and J.R. Arnold, $^{26}$Al depth profiles in Apollo 15 drill core, Earth Planet. Sci. Lett. 70, 164–168, 1984b.
25 J. Klein, R. Middleton and H. Tang, Modifications of an FN tandem for quantitative $^{10}$Be measurement, Nucl. Instrum. Methods 193, 601–616, 1982.
26 R. Middleton, J. Klein, G.M. Raisbeck and F. Yiou, Accelerator mass spectrometry with $^{26}$Al, Nucl. Instrum. Methods 218, 430–438, 1983.
27 D. Lal and B. Peters, Cosmic ray produced radioactivity on the earth, in: Handbuch der Physik, Vol. XLVI/2, Springer, Berlin, pp. 551–612, 1967.
28 W. Hampel, J. Takagi, K. Sakamoto and S. Tanaka, Measurement of muon-induced $^{26}$Al in terrestrial silicate rock, J. Geophys. Res. 26, 3757–3760, 1975.
29 T. Kirsten and W. Hampel, Weak radioactivities induced by cosmic ray muons in terrestrial minerals, Proc. Int. Conf. Low Radioactivity Measurements and Applications, Bratislava, 1977, 427–435, 1977.
30 Y. Yokoyama, J. Reyss and F. Guichard, Production of radionuclides by cosmic rays at mountain altitudes, Earth Planet. Sci. Lett. 36, 44–50, 1977.
31 K. Nishiizumi, C.P. Kohl, E.M. Shoemaker, J.R. Arnold, D. Lal, J. Klein, D. Fink and R. Middleton, *In situ* $^{10}$Be-$^{26}$Al exposure ages at Meteor Crater, Arizona, Lunar

Planet. Sci. XX, (Lunar Planet. Inst., Houston), 792–793, 1989.
32 F. Nishio and J.O. Annexstad, Glaciological survey of the bare ice area near the Allan Hills in Victoria Land, Antarctica, Mem. Natl. Inst. Polar Res., Spec. Issue 15, 13–23, 1979
33 J.O. Annexstad and L. Schultz, The 1988/89 remeasurement of the triangulation network at the Allan Hills Main Icefield, Victoria Land, Antarctica, Meteoritics 24, 248, 1989.
34 G. Delisle, J. Sievers and L. Schultz, Radio echo sounding (RES) survey across the Allan Hills Icefield, Antarct. J. U.S., submitted, 1989.
35 G.H. Denton, M.L. Prentice, D.E. Kellogg and T.B. Kellogg, Late tertiary history of the Antarctic ice sheet: Evidence from the Dry Valleys, Geology 12, 263–267, 1984.
36 R. Weed, Chronology of chemical and biological weathering of cold desert sandstones in the Dry Valleys, Antarctica, M.S. Thesis, University of Maine, 1985.
37 I.B. Campbell and G.G.C. Claridge, Landscape evolution in Antarctica, Earth Sci. Rev. 25, 345–353, 1988.
38 M.C. Malin, Abrasion in ice-free areas of southern Victoria Land, Antarctica, Antarct. J. U.S. 22(5), 38, 1987.
39 F.-D. Miotke, Formation and rate of formation of ventifacts in Victoria Land, Antarctica, Polar Geogr. Geol. 6(2), 90–113, 1982.
40 C.D. Ollier, G.F.M. Gaunt and I. Jurkowski, The Kimberley Plateau, Western Australia. A Precambrian erosion surface, Z. Geomorphol. N.F. 32-2, 239–246, 1988.